JOURNAL OF GEOPHYSICAL RESEARCH, VOL. 106, NO. A12, PAGES 30,337–30,348, DECEMBER 1, 2001

HiTIES: A High Throughput Imaging Echelle Spectrogragh for ground-based visible airglow and auroral studies

S. Chakrabarti, D. Pallamraju, and J. Baumgardner

Center for Space Physics, Boston University, Boston, Massachusetts, USA.

J. Vaillancourt

Department of Astronomy and Astrophysics, University of Chicago, Chicago, Illinois, USA.

Abstract. We describe an imaging spectrograph with high spectral resolution (0.3 Å) that uses an echelle grating without the conventional cross disperser. The spectrograph covers the entire visible region. However, only 5 - 20 wavelength regions can be observed simultaneously. The total wavelength coverage is limited by the number of available pixels on the detector and for a 1024 x 1024 pixels detector is $\sim$ 100 - 300 Å. Order separation is achieved by a mosaic of interference filters located at the image plane.

1. Introduction

Many interesting dynamically varying phenomena occur in the Earth's upper atmosphere. In the low and equatorial latitudes, strong electrodynamically coupled phenomena occur owing to the unique geometry of the magnetic field lines. In high latitudes the upper atmosphere is electrically coupled to the currents of magnetospheric origin. The coupling between various latitudinal locations becomes more pronounced during magnetic storms and substorms when there is a significant transfer of energy and momentum from the high to low latitudes (via traveling ionospheric disturbances, gravity waves, mapping of electric fields, etc.). All these geophysical phenomena leave different observable signatures.

One of the important and very useful means of investigating the upper atmospheric dynamics is by simultaneously measuring the optical airglow/auroral emissions that occur at different wavelengths. Airglow or auroral emissions originate owing to the de-excitations of electronic states (in case of atoms) and vibrational/rotational levels (in case of molecules) of the Earth's atmosphere. Hence the emission variabilities yield information on the atmospheric properties. Different emissions originate at different altitudes depending on the energies required for individual reactions and the number densities of the reactants at the given altitude. Therefore optical remote sensing at multiple wavelengths yields useful information on vertical propagation of waves and related effects. Furthermore, as different reactions require different energies for excitation, simultaneous measurement of different emission intensities yield useful information on the energetics of the incident particles, especially in the high-latitude regions. Of the various modes of measurements from different platforms (ground-based and space-based), ground-based measurements provide information on the temporal evolution of a phenomenon over a fixed site and ideally compliment the global measurements provided by the satellite-borne experiments. Also, ground-based measurements can employ larger integration times to observe weak emissions. Owing to this advantage, there have been many innovations made in the ground-based airglow observational techniques. We briefly highlight some approaches to compare them to the spectrograph presented in this paper.

Different techniques have been used earlier for nighttime airglow and auroral measurements. High-resolution Fabry-Perot scanning spectrometers have been used to obtain thermospheric neutral winds and temperatures by measuring O I 6300 Å emission line profile [see, e.g., *Shepherd et al.*, 1978; *Hernandez*, 1982; *Biondi et al.*, 1985; *Meriwether et al.*, 1986; *Sridharan et al.*, 1991]. These techniques essentially used a central aperture scanning method. Observations from different regions of the sky were accomplished by using a scan mirror pointed at different directions, which results in low temporal resolution when one needs to measure wind systems in all directions. With the advent of two-dimensional detectors, Fabry-Perot fringes are now imaged to obtain high-resolution wind and temperature measurements from a wide field of view (all-sky in most cases) [see, e.g., *Sivjee et al.*, 1980; *Rees and Green-*

Paper number 2001JA001105.
0148-0227/01/2001JA001105$09.00.

way, 1983; *Sekar et al.*, 1993; *Sridharan et al.*, 1993; *Biondi et al.*, 1995; *Conde and Smith*, 1995, 1997]. As many fringes are imaged at the same time, the "instantaneous" wind and temperature fields in a wide spatial region could be obtained with better time resolution than the central aperture scanning method. All these high-resolution measurments were made at the oxygen line at 6300 Å as it is bright and thermalized so that its doppler width is proportional to the ambient temperature. Using just an all-sky lens with a filter and a two-dimensional detector, one can obtain the intensity variation of a particular emission in all directions (180° × 180°). In this method, emissions from different wavelengths can be obtained using a filter wheel. Such measurements have been useful in obtaining plasma depletions from low latitudes, observing gravity wave propagations in various emissions, monitoring the movement of high-latitude plasma density enhancements, called plasma patches, etc. [e.g., *Mende et al.*, 1977; *Mendillo and Baumgardner*, 1982; *Weber et al.*, 1984; *Taylor et al.*, 1995]. To increase the throughput of the optical transmission of a spectrograph, *Mende et al.* [1993] employed a Hadamard mask containing multiple input slits in conjunction with an array detector. Using laboratory tests, they showed that the pattern of the image obtained can be deconvolved to retrieve the original spectrum. While this technique would work for a low light level background, it would not be efficient for higher background levels, such as in the twilighttime.

For all the techniques mentioned above, measurements at different wavelengths can be made only sequentially. Using a densely ruled grating and grism (grating-prism) respectively, spectral information in the whole visible wavelength range was obtained by *Baumgardner et al.* [1993] and *Swenson et al.* [1998]. Owing to a wide wavelength coverage of around 5000 Å and a finite number of detector elements, it is not possible to obtain finer details of the spectral features using such spectrographs.

In this paper we describe a new method by which simultaneous measurements at different (noncontiguous) wavelengths can be accomplished over a wide field of view (up to all-sky along the orientation of the slit). This instrument is a long slit echelle spectrograph and is called High Throughtput Imaging Echelle Spectrograph (HiTIES). HiTIES uses a unique "mosaic" design of filters at its image plane by which different spectral orders are separated. As can be readily seen, it has many aeronomical applications, especially in high latitudes, where many prominent and intense emissions occur simultaneously.

2. Optical Design

Traditional imaging spectrographs disperse the spectrum in wavelength in a monotonically increasing or decreasing order. This works well when the instrument parameters are such that the entire spectral region of interest can be accommodated by the available number of pixels on the detector. However, when one wants to record spectral lines in the 4000 - 10,000 Å wavelength region simultaneously at 0.3 Å resolution, one would need at least 40,000 detector pixels in one dimension (assuming that at least two detector pixels are used for sampling a spectral bin with a dispersion of 0.15 Å pix^{-1}). As of now, no electronic detector can deliver 40,000 pixels in one dimension. Conventional imaging spectrographs can therefore observe only a portion of the visible spectral range at a given time at high resolution. To observe all relevant features, these instruments must step through the wavelength range, which results in a loss of temporal resolution.

Our solution to this problem is based on the premise that most aeronomy studies require simultaneous data from only a handful of specific spectral features. The HiTIES instrument has the ability to simultaneously image several (5 - 20) user selected spectral features located anywhere in the visible spectrum (4,000 – 10,000 Å), all at high resolution (0.29 Å at 5893 Å). This resolution makes it possible to separate closely spaced features in a crowded region of the spectrum. Also, in an effort to constrain overall costs, HiTIES uses only off-the-shelf optical components.

Figure 1 shows the optical layout of the HiTIES instrument, and Table 1 lists the optical elements of HiTIES along with their characteristics. The HiTIES instrument is modular and is composed of four independent units: the foreoptics, the grating, the optics/filter assembly, and the detector. The foreoptics consist of a camera lens (used as an objective lens which is shown in Figure 1 as a fish-eye lens), a slit, and a field lens. HiTIES is designed to allow the user to easily change the field of view of the instrument by changing the focal length of the objective lens in the foreoptics. Incident light enters through the objective lens which is focused onto the slit. A field lens redirects light onto the collimator; the collimated beam is then diffracted by the grating and is imaged at the plane of the mosaic filter (discussed in section 2.2), which is used to sort the diffraction orders and select the spectral lines. This spectrum is then reimaged onto a position sensitive detector. Two flat mirrors are used as folding optics for packaging purposes.

Originally, we used a long, straight input slit (up to 60 mm) to increase the etendue (throughput) of the spectrograph. However, one of the consequences of using long input slits is that the spectral lines imaged on the detector are curved (see Figures 2 and 7). This curvature is caused by the aberration due to off-axis diffraction of light passing through the long, angular length of the slit. This curvature in the spectral image causes two undesirable effects for the HiTIES instrument: On-chip binning in the spatial direction (for increased signal-to-noise, SNR) is limited, owing to the degradation in spectral resolution when more than a few pixels are binned (post read-out spatial binning can also be done, but in

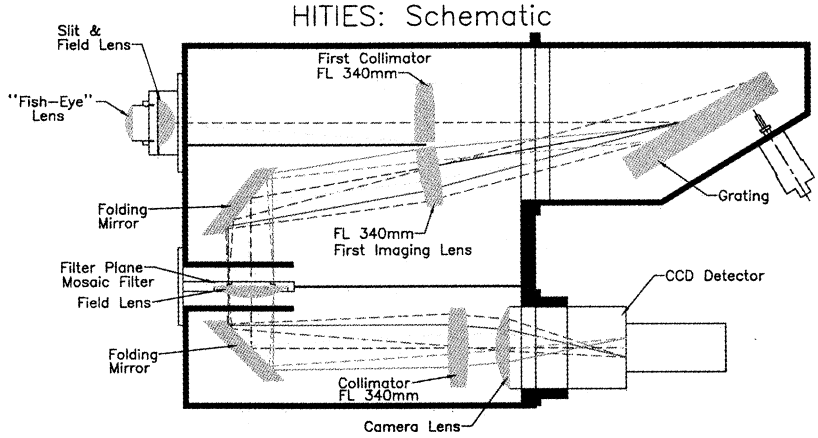

Figure 1. The optical layout of the High Throughput Imaging Echelle Spectrograph (HiTIES) instrument. At its heart are an echelle grating and a multipanel mosaic filter that replaces cross dispersers found in astronomical echelle systems. Other components include interchangeable foreoptics, folding mirrors, collimators, field and imaging lenses, and a two-dimensional imaging detector.

this case the read-out noises of the detector are added as well); if left uncorrected, the curved spectral lines would limit the width of the individual panels in the mosaic filter, allowing fewer wavelength regions to be sampled. Therefore we carried out a sequence of tests by using slits of varying curvatures. The results of these tests revealed that the use of a particular curvature in the input slit results in completely eliminating the curvature of the spectral lines at the image plane for a particular grating angle. However, as the spectra imaged on the detector are over an angle region of $\pm$ 4° from the central diffraction angle, it results in a finite amount of "overcompensation" and "undercompensation" of the curvature on either side of the correction wavelength along the dispersion direction (the shape being similar to pin-cushion distortion). Neverthless, the examples shown in Figures 12 and 13, obtained using a curved input slit, show that the effect of curvature has been reduced considerably (when compared to the schematic shown in Figure 7). In this case one could carry out on-chip binning both to improve the SNR of the measurement and to reduce the data volume and read-out time from the chip. The prototype HiTIES also suffers from chromatic aberration, which can be reduced by replacing the lenses by multi-element apochromatic lenses.

Although twilighttime measurements were made with a resolution of 2.3 Å (Figure 13), it was not possible to carry out unambiguous daytime measurements at multiple wavelengths, owing to the unavailability of a proper detector (as discussed further in section 3.2). For the specific purpose of carrying out daytime measurements we have developed another instrument (called HIRISE) that measures only one spectral band at a higher spec-

Table 1. Characteristics of HiTIES instrument[a]

Instrument Component	Description
Foreoptics	various (user selectable)
	slit: 60 mm × ∼ 20 – 500 μm
	field lens: planoconvex, ϕ = 60 mm, FL = 70 mm
First collimator and first imaging lens	f/3.4, FL = 340 mm
	1 inch cut-off edge to minimize aberrations
Grating	ruled area: 102 mm × 206 mm
	line spacing: 98.76 grooves/mm
	blaze angle: 63°26'
	incident angle: 58.5°
	angle between incident and exit beam: 10° fixed
Folding mirrors (flat)	elliptical telescope mirrors, minor axis = 80 mm
Multipanel filters	placed at image plane before field lens
Re-imaging optics	field lens: f/4, FL = 300 mm
	collimator: f/3.4, FL = 340 mm
	camera lens: f/1.2, FL = 85 mm
Detector	intensified or bare CCD
	effective pixel size: 24 μm

[a] HiTIES, High Throughput Imaging Echelle Spectrograph; FL, focal length.

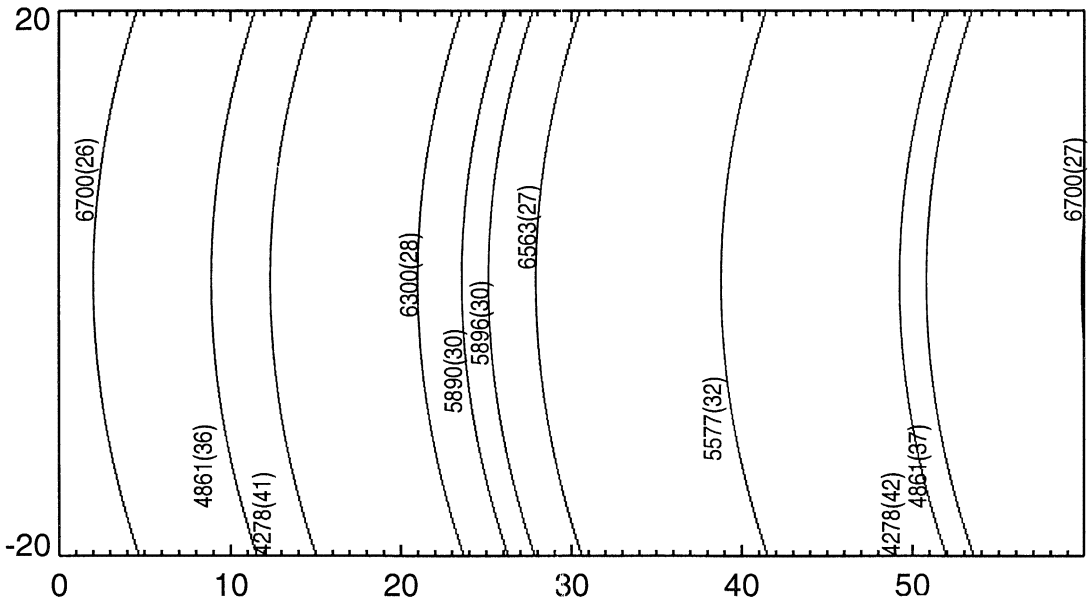

Figure 2. A ray trace computation showing the placement of several prominent airglow lines and some of the test lines used, at the image plane. The numbers in parentheses indicate the diffraction order in which the line occurs. Notice the severe curvature in the lines that are introduced as a consequence of using a long, straight input slit. This has been minimized by replacing the straight slit with a curved input slit (see text for details).

tral resolution [*Pallamraju et al.*, 2001b]. Using this instrument, the authors have reported on a comprehensive study of the Ring effect in the day sky spectrum [*Pallamraju et al.*, 2000] and on the detection of a daytime auroral arc from measurements carried out in Sondrestromfjord, Greenland [*Pallamraju et al.*, 2001a].

2.1. Choosing a Diffraction Grating

The choice of the diffraction grating is central to the design of any spectrograph and is best explained by examining the grating equation:

$$m\lambda = d(\sin\alpha + \sin\beta), \tag{1}$$

where m is the diffraction order, λ is the operating wavelength, d is the groove spacing or the inverse of the ruling density, and α and β are the incident and diffracted angles, respectively (see Figure 3 for the definition of the angles). HiTIES achieves high dispersion by using high diffraction orders (m ranging from 20 to 50). When using high orders, spectra from a number of different orders will be diffracted in the same direction, which results in order overlap. Note that (1) can be sat-

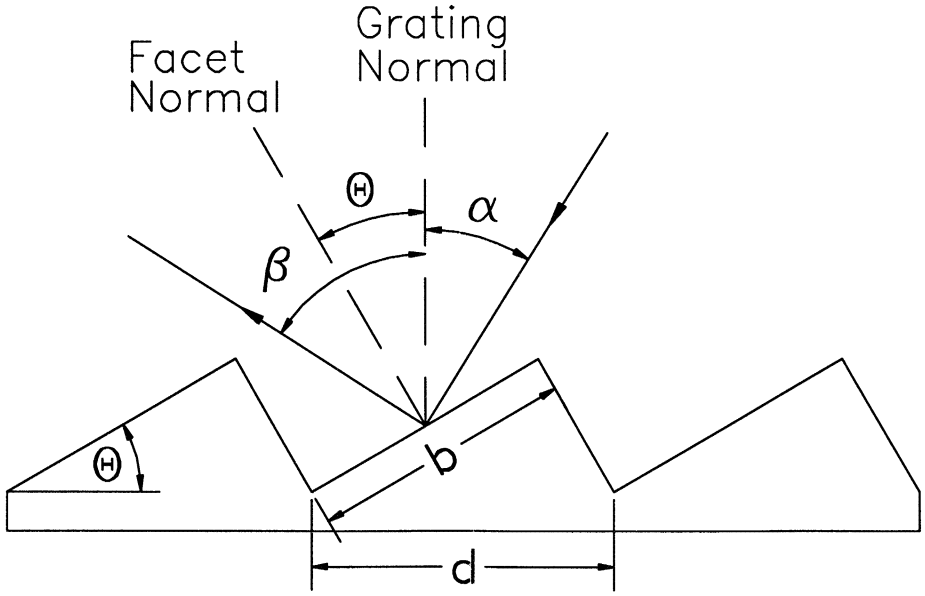

Figure 3. Grating geometry and the definition of the relevant parameters.

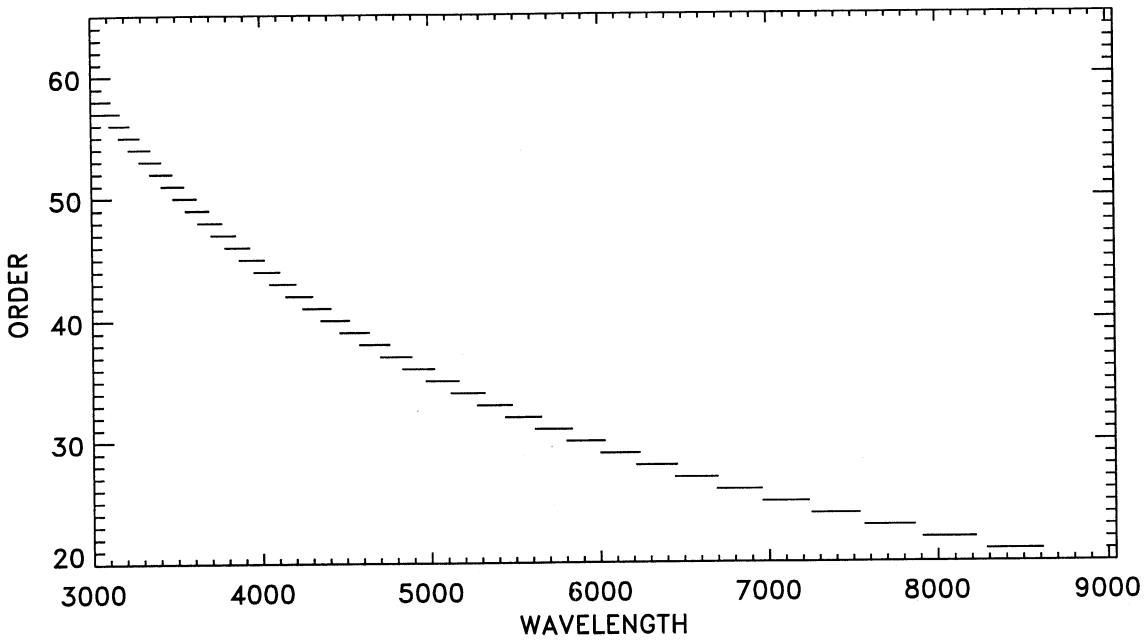

Figure 4. The wavelength range that will be diffracted into the given diffraction angle range for a given order, indicated by the horizontal bars. All the ranges in each order will appear simultaneously on the detector. Note that regions with wavelength gaps increase with increasing wavelength and decreasing diffraction order. A spectral feature is repeated if it occurs in more than one order and does not occur at all if it appears in a "gap" such as those that appear between 7000 and 9000 Å.

isfied by a combination of a range of wavelengths and orders for the same set of α and β (i.e., $m_1\lambda_1 = m_2\lambda_2$).

The degree of order overlap that occurs in spectrographs operating at high diffraction orders (see Figure 2) can be described by the free spectral range (Figure 4). The free spectral range is the range of wavelengths in a given diffraction order for which superposition of light from adjacent orders does not occur. Depending upon the order, the free spectral range of HiTIES is $\sim$ 100 – 300 Å. The high optical throughput of the spectrograph is achieved by operating the instrument as close to the blaze angle (θ) for the grating as possible. In the end the chosen parameters were a groove density of 98.7 lines mm^{-1} and a blaze angle of 63.5°.

The efficiency of the grating as a function of the incident and diffraction angles, as well as wavelength and diffraction order, is given by the blaze function. The blaze function determines the fraction of energy diffracted into a given order [*Schroeder*, 1987]:

$$BF = \frac{\sin^2\gamma}{\gamma^2}, \qquad (2)$$

$$\text{where} \quad \gamma = \frac{\pi b}{\lambda}(\sin\beta + \sin\alpha) \qquad b = d\cos\theta.$$

When using an echelle grating, the intensity of diffracted light falls off quickly away from the blaze angle as can be seen in Figure 5. Figure 6 shows a plot of grating efficiency (blaze function) versus wavelength for a number of diffraction orders in the Littrow mode ($\beta = \alpha$) for HiTIES. For all orders the efficiency falls to $\sim$ 40% in the free spectral range of that order.

The choice of the best incident angle (α) for the grating is made after putting the wavelengths of interest into a computer model of the instrument developed at Boston University. This model uses the grating equation and the range of diffracted angle that can be accommodated by the detector (typically around 8°) to determine the most suitable grating angle. This angle is a practical constraint of the ideal angle (where the blaze is centered on the detector) $\pm$ 4°. For higher orders ($N > 35$) there is considerable overlap, and a line may appear twice on the detector, while for low orders some line may not appear at all. A complement of lines for airglow and auroral studies at 6300 Å, 5577 Å, 4278 Å, H_α, and H_β have been chosen as a test case. From ray trace calculations it was determined that an incident angle of $\alpha = 58.5°$ would produce the most suitable placement of these features.

2.2. Order Separation

This "problem" of order overlap described earlier is the one that HiTIES uses to its advantage. This technique (of using overlapping orders) to obtain high dispersion would not be useful unless it is possible to separate the overlapping orders. When echelle spectrographs are used in astronomy, a cross-dispersing element (a prism or another grating) is used to separate the overlapping orders. In such applications the spectral orders can be stacked vertically on the detector and dis-

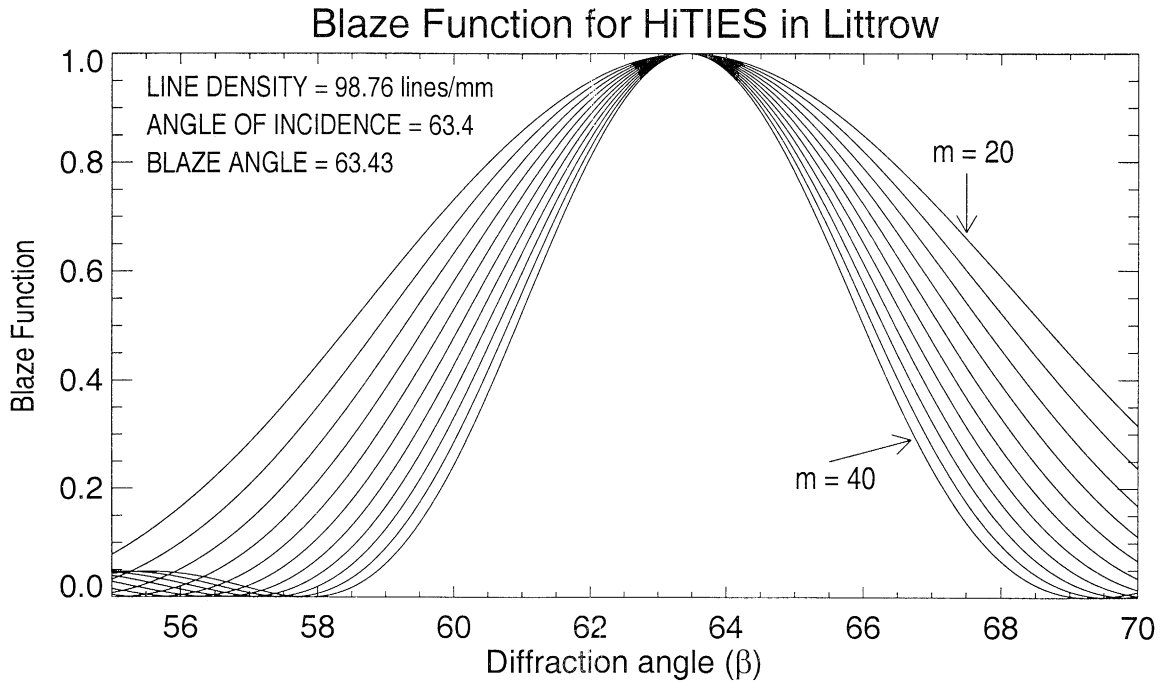

Figure 5. Grating blaze efficiency for different orders (20-40) plotted as a function of diffraction angle. It can be seen that the efficiency falls off rapidly away from the blaze angle independent of the wavelength.

persed horizontally across it. However, in imaging extended sources the slit image fills the vertical extent of the detector, so that a cross disperser is not an option. HiTIES utilizes a mosaic filter, which is composed of several windows of interference filters, one filter for each of the desired spectral features. Each of these interference filters is hard coated to deliver a peak transmission (of 70%) even at their edges, and each is cut to size after lamination. The individual strips of filters are reassembled to form a mosaic filter at the correct location as described by the computer model, which is then placed at the first image plane. The resulting spectrum is 40

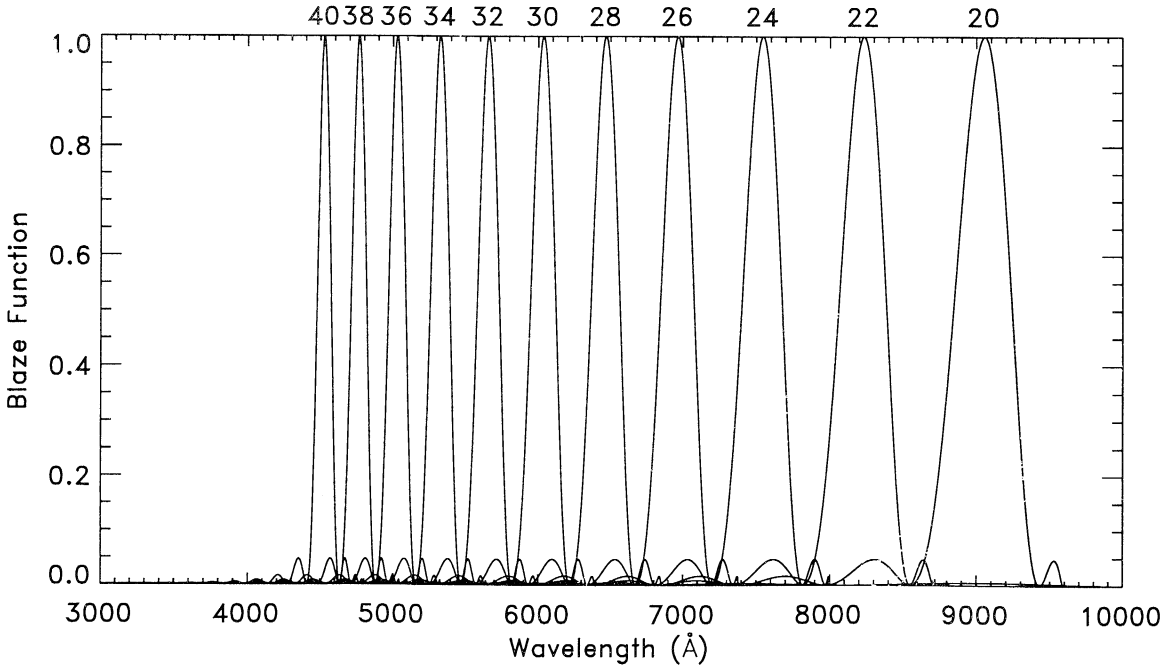

Figure 6. Grating blaze efficiency for diffraction orders 20 – 40 plotted as a function of wavelength. An efficiency of 1.0 is that found at wavelengths in the blaze direction in Littrow mode. The grating's efficiency falls to $\sim$ 40% of its peak within the free spectral range of each given order.

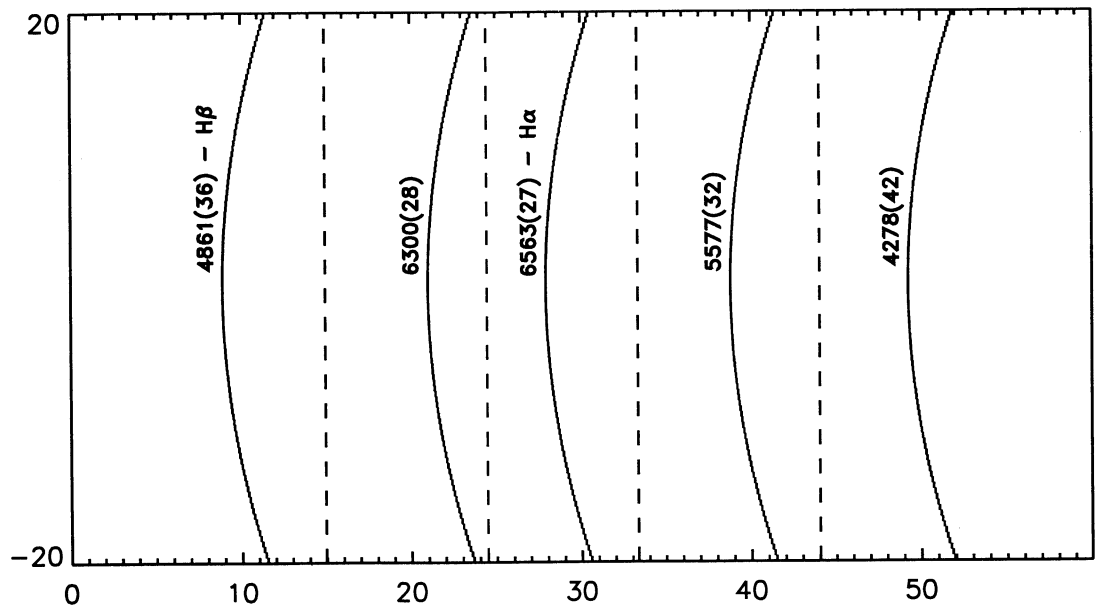

Figure 7. A ray trace plot using the same optical parameters as those in Figure 2 but with a five-panel mosaic filter inserted to pass only selected airglow features. The dashed vertical lines indicate the edges of the filter panels. Each panel is ~ 5–15 mm wide.

mm in spatial direction and 50 mm in spectral direction (coverage up to ~ 8° of dispersion). Figure 2 shows results of a ray trace calculation before the insertion of a mosaic filter, while Figure 7 shows ray trace results after inserting such a filter. These filters typically have much broader band pass (~ 100 - 200 Å full width at half maximum (FWHM)) than used in many coupling energetics and dynamics of atmospheric regions (CEDAR) imaging applications where typical filter band passes are < 10 Å.

In order to separate the orders in this way, the mosaic filter must be placed at or near the focal plane in a converging beam of light. Because the filters have a finite thickness, this produces a "shadow zone" at the boundaries of the filter panels which reduces the throughput (see Figure 8). On the other hand, these shadow zones provide an estimate of background signal during the observations and can be used for quantitative estimates of the observed signal. We expect that an upper limit to the number of panels that could be used is ~ 20 for the 50 mm square filters used by the instrument (assuming 2 mm of clear area and 0.6 mm of shadow zone for each filter panel).

3. Test Results

3.1. Experimental Confirmation of Ray Traces

The ray traces produced in Figures 2 and 7 were confirmed experimentally on a laboratory optical bench before constructing the instrument. Sodium and hydrogen lamps were used to compare the placement of some of their spectral features to those from our ray trace. The results are shown in Figure 9.

3.2. Spectral Resolution

Several tests of HiTIES resolution were made with the sodium doublet at 5890 and 5896 Å, in the 31st order (31st order is closer to the blaze angle for $\alpha \sim 60°$, for these features than the 30th order shown in Figure 2). Slits of width 20, 130, and 530 μm were used for tests with the instrument in the optical configuration shown in Figure 1. Using the Rayleigh criteria, the resulting resolutions were 0.29 Å for for the 20 μm slit, 0.9 Å for the 130 μm slit, and 2.3 Å for the 530 μm slit, respectively. The theoretical resolutions for these slit widths are 0.12, 0.64, and 2.6 Å, respectively. The discrepancy between the measured and calculated resolutions (especially why one measurement is greater than the calculation and the others are smaller) is most likely due to the choice of α and β used for the calculations. Figure 10 shows an example of the spectrum recorded by the instrument at the highest resolution reported here.

Throughput is best measured in terms of the system's efficiency. Preliminary estimates of HiTIES end-to-end efficiency (of optics) have yielded a value of 20% in the visible region. However, the measurements are further dependent on the quantum efficiency of the detector used, since one can easily change to a detector having a different quantum efficiency. Therefore it is more useful to examine the system's luminosity (the effective area-solid angle product). The luminosity is found using 20% as the system's optical efficiency and the chosen instrument characteristics given in Table 1. The calculated luminosities for the three resolution tests performed are given in Table 2.

For the laboratory and field tests reported in this paper we used an intensified CCD (ICCD) as the detector,

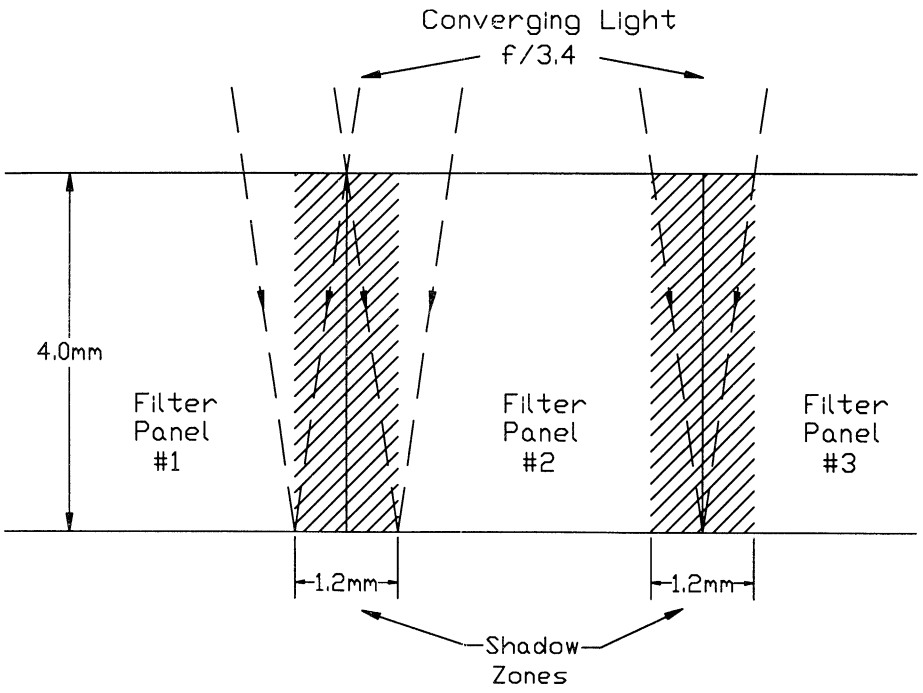

Figure 8. Three adjacent filter panels intercepting converging beams of light. The throughput will be reduced at the edges of the panels because some of the rays in the $f/3.4$ light cone are unable to penetrate the entire thickness (4 mm) of the filter before hitting the filter edge, thus resulting in a "shadow zone." The shadow zone has a width of 1.2 mm for the instrument configuration presented here.

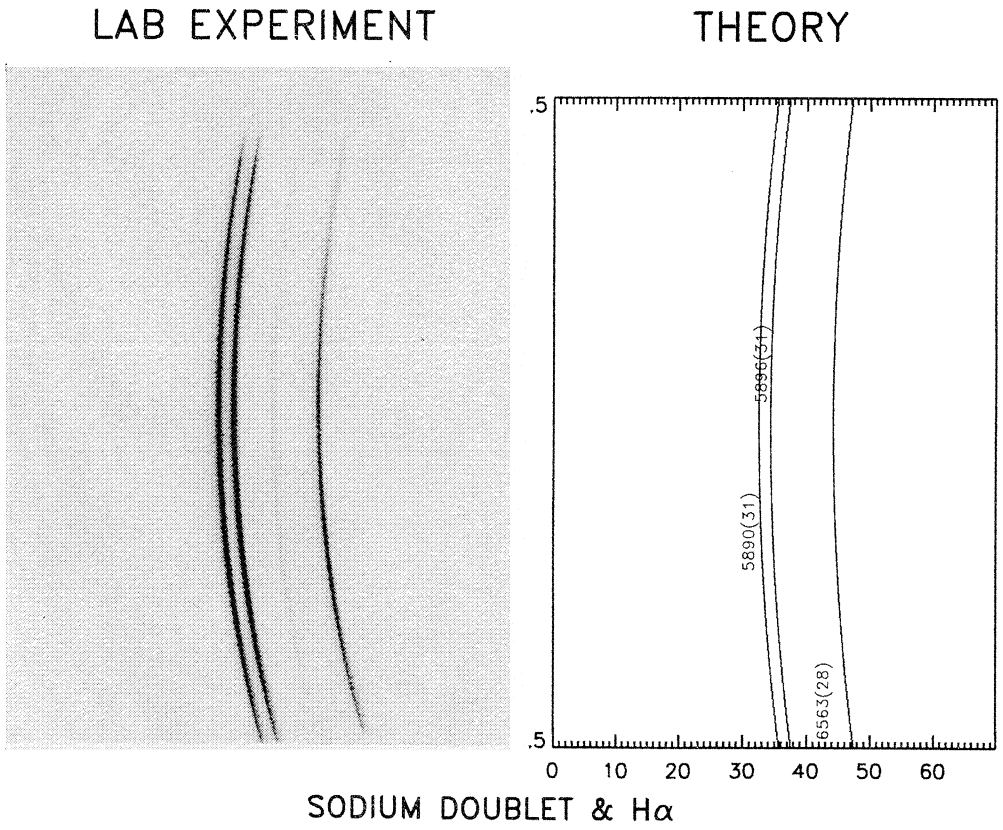

Figure 9. (Left) The experimental image obtained in the laboratory using sodium and hydrogen lamps as light sources. (Right) The results of our ray trace calculations for comparison.

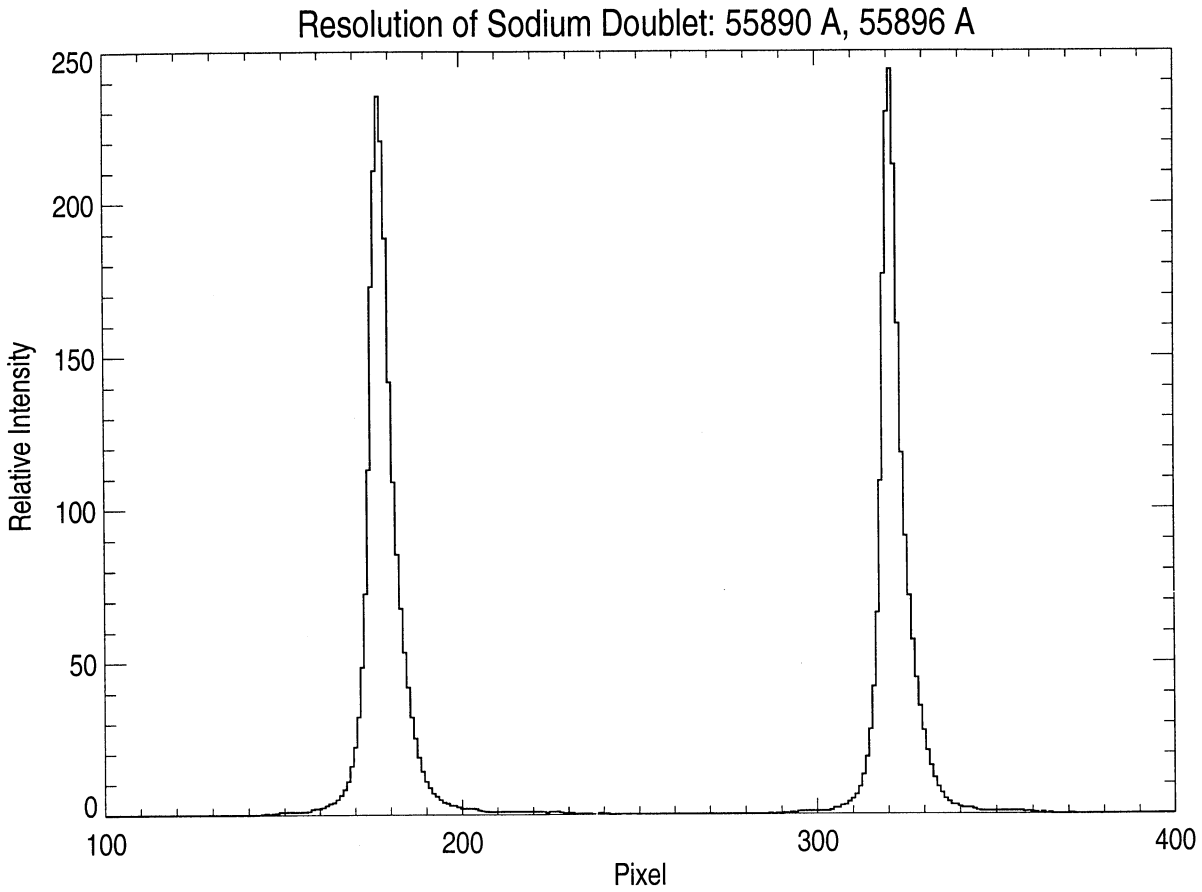

Figure 10. Line profile from an image of a sodium lamp with a 20 μm slit. The full width at half maximum (FWHM) of each of the lines in sodium doublet (located at $\sim$ 5890 and 5896 Å) is $\sim$ 7 pixels, while their separation is $\sim$ 145 pixels. The resulting resolution (FWHM) is therefore $\sim$ 0.29 Å.

which has a quantum efficiency (QE) of around 15%. The ICCD was the only detector available to us for use with this instrument. As the detector's QE is small and its number of resolution elements were less than optimum, we increased the slit width for increasing the throughput and used the low-resolution (2.3 Å) set-up to study nightglow and twilighttime airglow. For the daytime applications we plan to use a bare CCD which has higher QE (around 80%) and more resolution elements so that we can reduce the slit width to obtain a higher resolution (of 0.3 Å).

3.3. Field Tests

HiTIES's first field test was conducted without a mosaic filter. Figure 11 shows an image taken of the night sky. A 5577 Å filter was placed on the top portion of the filter plane while the bottom portion had no filter. The bottom portion of the image contains airglow emission lines from the night sky, including 5577 and 6300 Å from oxygen emission as well as the broad scattered background continuum. The top portion clearly shows that only the 5577 Å feature was transmitted through the filter. Note that the scattered continuum feature virtually disappeared.

To test the suitability of this instrument for aeronomy studies, the instrument was deployed at the Boston University's optical site at the Millstone Hill Observatory. The instrument was equipped with a 35 mm focal length lens as its foreoptics and a four-panel filter system to observe the O I 5577 and 6300 Å features

Table 2. The Luminosities and RL Products Estimated From the Given Instrument Characteristics and the Slits and Detectors Used in the Three Resolution tests[a]

Slit Width; μm	Pixel Size; μm	f_{cam}; mm	Calculated L; cm^2 sr^{-1}	Calculated $R(\lambda/\Delta\lambda)$	Measured R	Estimated RL Product
20	24	340	9.04×10^{-5}	50,000	20,000	1.8
130	24	85	5.88×10^{-4}	9,300	6,500	3.82
530	24	85	2.392×10^{-3}	2,300	2,600	6.21

[a] The luminosities assume a 20% system efficiency. L, Luminosity; R, Resolution.

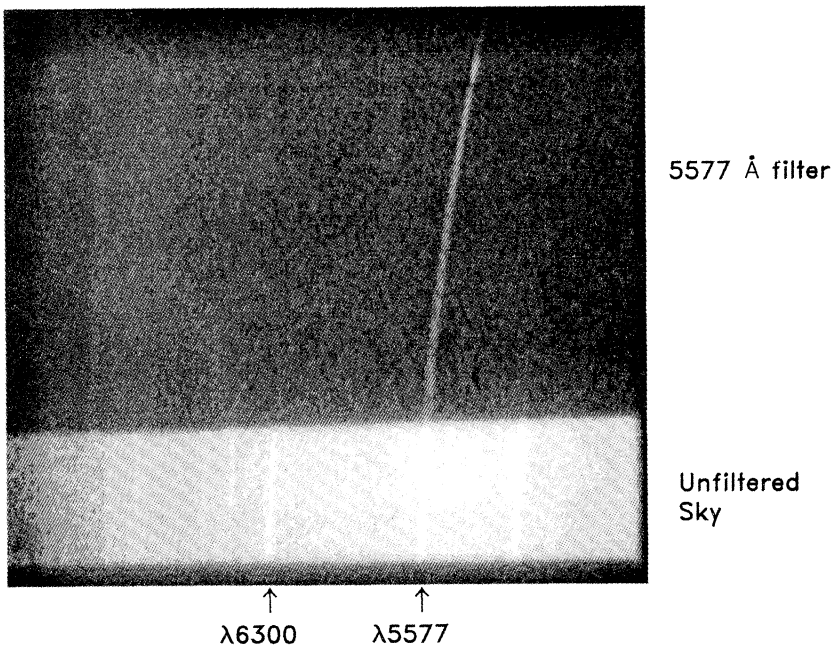

Figure 11. Image of the night sky. The top section of the image was filtered with a 150 Å (FWHM) 5577 Å filter. The bottom portion of the image is unfiltered. The 6300 Å line of oxygen is also visible in this part.

as well as H_α and H_β lines. Figure 12 shows data obtained around 0345 UT on December 3, 2000, that show the oxygen features. In this image the x axis represents dispersion direction at different wavelength panels as described earlier. Owing to the imaging property of HiTIES, different sections on the y axis of this image can be mapped to different spatial regions on the sky with a knowledge of the emission altitude of each wavelength. The 5577 and 6300 Å airglow emissions can be clearly seen all through the slit orientation. Figure 12

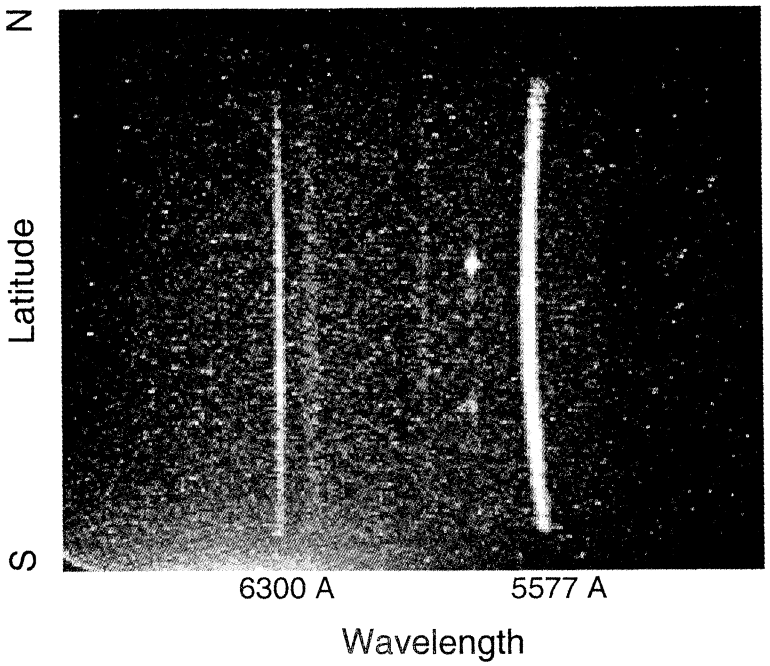

Figure 12. Spectral image of the night sky obtained at 0345 UT on December 3, 2000, at the Millstone Hill Observatory. A four-panel filter and a 35 mm lens were used. The 5577 and 6300 Å lines of atomic oxygen can be seen in this image. Proton-induced emissions can also be seen left of the 5577 Å emission region.

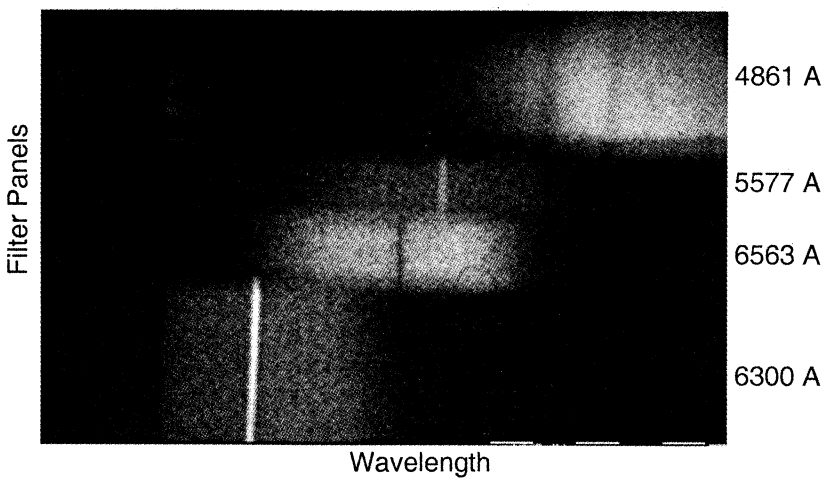

Figure 13. Twilighttime spectral image obtained from Sondrestromfjord, Greenland, at 1144 UT (0844 LT) on January 18, 2001. The same filter panel that was used for obtaining Figure 12 was used here as well. However, its orientation is perpendicular to that of the slit. Different wavelength panels are marked on the figure. Such an arrangement is useful especially in cases where large Doppler shifts are expected. Note the simultaneous presence of Fraunhofer absorption lines and emissions (in different wavelength panels) indicating observations of sunlit aurora. The dark boundaries between different wavelength panels are the shadow zones discussed in section 2.2.

also shows a bright patch $\sim$ 5 km in size (left of 5577 Å), possibly of galactic origin, which moved toward north during the course of our observations. A closer inspection also reveals the presence of a fainter signal filling the entire slit at this spectral region. This is most probably the signature of proton aurora at 6563 Å.

Figure 13 shows a sample data obtained using HiTIES from Sondrestromfjord, Greenland. This image was obtained during the morning twilighttime at 1144 UT (0844 LT) on January 18, 2001. The scientific objective here was to observe both proton-and electron-induced auroras simultaneously. Proton emissions are known to be blue shifted at these latitudes. To avoid "loosing" the proton emission features for the extreme drifts (of $\sim$ 30 Å), we placed the mosaic filter perpendicular to the slit orientation, unlike the "normal" usage, as shown in Figure 12. Different wavelength panels used are labeled on the right. This arrangement allows practically the whole of the CCD area (in spectral direction) available for even extreme Doppler shifts in proton emissions. The 4861 and 6563 Å filter panels have larger band pass as compared to the 5577 and 6300 Å panels. Note that this is another feature of HiTIES by which one can use different bandwidths for different wavelength panels as required by the the scientific objective. Solar spectrum has strong absorption lines at H_α and H_β; one can notice the absorption features at these two panels in comparison to the scattered solar background continuum. The emission lines at 5577 and 6300 Å can also be seen in Figure 13. If the objective lens in the front end had a large focal length, the spatial regions mapped on to the sky between the various wavelengths would not be too separated from one another. This observation clearly demonstrates that the 5577 and 6300 Å emission features were obtained while the Fraunhofer features were present in the sky during the twilighttime. HIRISE instrument [*Pallamraju et al.*, 2001b] takes over from this instrument to make daytime observations. Optical observations as shown in Figure 13 demonstrate the versatility of the applications using HiTIES.

The column-integrated airglow emission rates measured by HiTIES (as shown in Figures 12 and 13) can be plotted as a function of time to investigate temporal evolution/modulation in the emission rates at different latitudes and at various wavelengths simultaneously. As pointed out earlier, such an observation would help in understanding the causative mechanisms of these emissions, which are a consequence of the dynamics of the region of their origin. Detailed analysis of both the campaign's data is underway, and the science results will be presented elsewhere.

4. Summary

We have presented an imaging spectrograph with high spectral resolution and high throughput. Its innovativeness lies in the fact that it presents a new capability of measuring spectral characteristics from (noncontiguous) multiple wavelengths simultaneously at resolutions sufficient for obtaining information on integrated airglow intensities and Doppler shifts for emitting particles moving with high velocities, such as in the case of H_α and H_β. The required characteristics for such an instrument were theoretically examined with ray trace calculations and compared against the performance of

a prototype instrument. This instrument's capabilities have been demonstrated both in the laboratory and in the field. HiTIES has currently achieved a resolution of 0.29 Å at the sodium doublet, corresponding to a resolving power (R) of $\lambda/\Delta\lambda = 20,000$. Preliminary estimates yield a system efficiency of 20%. Field tests at 2.3 Å resolution show that the instrument is capable of observing several airglow and auroral features simultaneously, all at high spectral resolution.

Acknowledgments. We are grateful to Valerie Taylor and Andrew Stephan for their help with the manuscript. We are also indebted to Joei Wroten for her help with data reduction. This work was supported by NSF grant ATM 9601846 and USRA Student Explorer Demonstration Initiative (STEDI) grant 1500-05.

Janet G. Luhmann thanks the referees for their assistance in evaluating this paper.

References

Baumgardner, J., B. Flynn, and M. Mendillo, Monochromatic imaging instrumentation for applications in aeronomy of the Earth and planets, *Opt. Eng., 32*, 3028-3032, 1993.

Biondi, M. A., D. P. Sipler, and M. Weinschenker, Multiple aperture exit plate for field-widening a Fabry-Perot interferometer, *Appl. Opt., 24*, 232-236, 1985.

Biondi, M. A., D. P. Sipler, M. E. Zipf, and J. L. Baumgardner, All-sky Doppler interferometer for thermospheric dynamics studies, *Appl. Opt., 34*, 1646-1654, 1995.

Chakrabarti, S., Ground-based spectroscopic studies of sunlit airglow and aurora, *J. Atmos. Sol. Terr. Phys., 60*, 1403-1423, 1998.

Conde, M., and R. W. Smith, Mapping thermospheric winds in the auroral zone, *Geophys. Res. Lett., 22*, 3019-3022, 1995.

Conde, M., and R. W. Smith, Phase compensation of a separation scanned, all-sky imaging Fabry-Perot spectrometer for auroral studies, *Appl. Opt., 36*, 5441-5450, 1997.

Hernandez, G., Analytical description of a Fabry-Perot spectrometer 7: TESS, a high-luminosity high-resolution twin-etalon scanning spectrometer, *Appl. Opt., 21*, 507-513, 1982.

Mende, S., R. H. Eather, and E. K. Aamodt, Instrument for monochromatic observations of all sky auroral images, *Appl. Opt., 16*, 1691-1700, 1977.

Mende, S. B., E. S. Claflin, R. L. Rairdon, and G. R. Swenson, Hadamard spectroscopy with a 2 dimensional detector array, *Appl. Opt., 32*, 7095-7105, 1993.

Mendillo, M., and J. Baumgardner, Airglow characteristics of equatorial plasma depletions, *J. Geophys. Res., 87*, 7641-7653, 1982.

Meriwether, J. W., Jr., J. W. Moody, M. A. Biondi, and R. G. Roble, Optical interferometric measurements of nighttime equatorial thermospheric winds at Arequipa, Peru, *J. Geophys. Res., 91*, 5557-5566, 1986.

Pallamraju, D., J. Baumgardner, and S. Chakrabarti, A multiwavelength investigation of the Ring effect in the day sky spectrum, *Geophys. Res. Lett., 27*, 1875-1878, 2000.

Pallamraju, D., J. Baumgardner, S. Chakrabarti, and T. Pedersen, Simultaneous ground-based observations of an auroral arc in daytime/twilighttime OI 630.0 nm emission and by incoherent scatter radar, *J. Geophys. Res., 106*, 5543-5549, 2001a.

Pallamraju, D., J. Baumgardner, and S. Chakrabarti, HIRISE: A ground-based High Resolution Imaging Spectrograph using Echelle grating for measuring daytime airglow/auroral emissions, *J. Atmos. Sol. Terr. Phys.*, 2001b (in press).

Rees, D., and A. H. Greenway, Doppler imaging system: An optical device for measuring vector winds, 1: General principles, *Appl. Opt., 22*, 1078-1083, 1983.

Schroeder, D. J., *Astronomical Optics*, Academeic, San Diego, Calif., 1987.

Sekar, R., S. Gurubaran, and R. Sridharan, All-sky imaging Fabry-Perot spectrometer for investigation of the upper atmosphere, *Ind. J. Radio Space Phys., 22*, 197-204, 1993.

Shepherd, G. G., A. J. Deans, and Y. P. Neo, SCIMP: A scanning interferometric multiplex photometer, *Can. J. Phys., 56*, 681-686, 1978.

Sivjee, G. G., T. J. Hallinan, and G. R. Swenson, Fabry-Perot imaging system for thermospheric temperature and wind measurements, *Appl. Opt., 19*, 2206-2209, 1980.

Sridharan, R., S. Gurubaran, R. Raghavarao, and R. Suhasini, Coordinated thermospheric and F-region measurements from low latitudes, *J. Atmos. Terr. Phys., 53*, 515-519, 1991.

Sridharan, R., R. Sekar, and S. Gurubaran, Two-dimensional high resolution imaging of the equatorial plasma fountain, *J. Atmos. Terr. Phys., 55*, 1661-1665, 1993.

Swenson, G. R., R. L. Raidern, S. C. Solomon, and S. Ananth, Imaging spectrometry for 2 dimensional characterization of auroral emissions, *Appl. Opt., 37*, 5740-5770, 1998.

Taylor, M. J., M. B. Bishop, and V. Taylor, All-sky measurements of short-period waves imaged in the OI (557.7 nm), Na (589.2 nm) and near-infrared OH and $O_2(0,1)$ nightglow emissions during the ALOHA-93 campaign, *Geophys. Res. Lett., 22*, 2833-2836, 1995.

Weber, E. J., J. Buchau, J. G. Moore, J. R. Sharber, R. C. Livingston, J. D. Winningham, and B. W. Reinisch, F layer ionization patches in the polar cap, *J. Geophys. Res., 89*, 1683-1694, 1984.

J. Baumgardner, S. Chakrabarti, and D. Pallamraju, Center for Space Physics, 725 Commonwealth Avenue, Boston University, Boston, MA, 02215, USA. (jeff@spica.bu.edu; supc@bu.edu; dpraju@bu.edu)

J. Vaillancourt, University of Chicago, Dept. of Astronomy and Astrophysics, 5640 S. Ellis, Chicago, IL 60637, USA. (johnv@oddjob.uchicago.edu)

(Received January 16, 2001; revised July 11, 2001; accepted July 13, 2001.)